Accelerated Thermal Aging Effects on Carbon-based Perovskite Solar Cells: a Joint Experimental and Theoretical Analysis.

*Giovanni Pica, Matteo Degani, Giorgio Schileo, Alessandro Girella, Chiara Milanese, David Martineau, Lucio C. Andreani, Giulia Grancini**

G. Pica, M. Degani, Dr. G. Schileo, Dr. A. Girella, Prof. C. Milanese, Prof. G. Grancini

Department of Chemistry and INSTM, University of Pavia, Via T. Taramelli 14, 27100 Pavia, Italy

E-mail: giulia.grancini@unipv.it

Dr. D. Martineau

Solaronix S.A., Rue de l'Ouriette 129, Aubonne 1170, Switzerland

Prof. L. C. Andreani

Department of Physics, University of Pavia, Via A. Bassi 6, 27100 Pavia, Italy

Keywords: Perovskite solar cell, thermal stress, efficiency, solar cell stability, fitting

Abstract. In the search for stable perovskite photovoltaic technology, Carbon-based Perovskite solar cells (C-PSCs) represent a valid stable solution for near future commercialization. However, a complete understanding of the operational device stability calls for assessing the device robustness under thermal stress. In this work, we monitor the device response upon a prolonged thermal cycle aging (heating the device for 1 month up to 80°) on state-of-the-art C-PSCs, often neglected, mimicking outdoor conditions. We combine device characterization and in house developed advanced modelling of the current–voltage characteristics of

the C-PSCs by using an iterative fitting method based on the single-diode equation to extrapolate series (R_S) and shunt resistances (R_{SH}). Two temperature regimes have been identified: below 50°C C-PSCs are stable, while switching to 80°C a slow device degradation takes place. This is associated to a net decrease of the device R_{SH}, while the R_S is unaltered, pointing to interface deterioration. Indeed, structural and optical analysis, by means of X-ray diffraction and photoluminescence studies, reveal no degradation of the perovskite bulk, providing clear evidence that perovskite/contacts interfaces are the bottleneck for thermal-induced degradation in C-PSCs.

Introduction

Within the field of modern photovoltaics (PV), hybrid perovskite solar cells far outstripped the most of current technologies, with their power conversion efficiency (PCE) reaching 25% and beyond with unprecedented speed.[1] Device instability, caused by humidity, exposure to oxygen or UV light, high temperature, and electrical bias, must be tackled.[2-10] Increasing the robustness of PSCs calls for multiple routes: from improving the perovskite crystallinity itself,[11] to designing protective layers – as for instance low dimensional perovskites,[12] transition metal dichalcogenide[12-14] or inorganic films,[15] to optimizing the full device architecture. Despite being widely used, metal contacts, for instance, induce metal infiltration in the perovskite bulk,[16] and hamper device stability. Carbon based perovskite solar cells (C-PSCs), known for being a long-term stable and cheap alternative – where carbon substitutes the top electrode - hold the potential for a breakthrough marketable solution.[17-20] Replacing the organic hole transporting material and the top metal contact with carbon limits the instabilities, delaying the degradation of the device. This is particularly true at operating temperatures

above 70°C.[21] Thermal stress is indeed affecting device degradation,[3] often underestimated when considering the operational stability of the cells. In this work, we address this issue, monitoring the effect of thermal aging on state-of-the-art C-PSCs, by imposing a prolonged (27 days) temperature cycling stress, with the intend to mimic outdoor conditions. The measured device current-voltage characteristics have been modelled by an advanced iterative fitting method, based on the single-diode equation with series (R_S) and shunt resistances (R_{SH}). Below 50°C C-PSCs are stable, while switching to 80°C a slow device degradation takes place. The fitting model suggests the reason behind assigned to a net decrease of the device R_{SH}, while the R_S is unaltered. This suggests that deterioration starts from interfacial contacts, while further structural and morphological analysis reveal no degradation of the perovskite bulk layer.

Results and discussion

A series of semi-encapsulated C-PSCs (sandwiched between two sheets of glass and an encapsulant but without an edge sealant) were measured under a defined aging protocol consisting of a temperature cycle between 50° and 80°, keeping a relative humidity RH=72%. The temperature regimes chosen are respectively below and above the phase transition temperature of the active material, that occurs around 54° and it is fully reversible. The test was run for 648 hours (27 continuous days) alternating between stress and recovering periods, as indicated in the by the red and blue slots in the caption of **Figure 1a**.

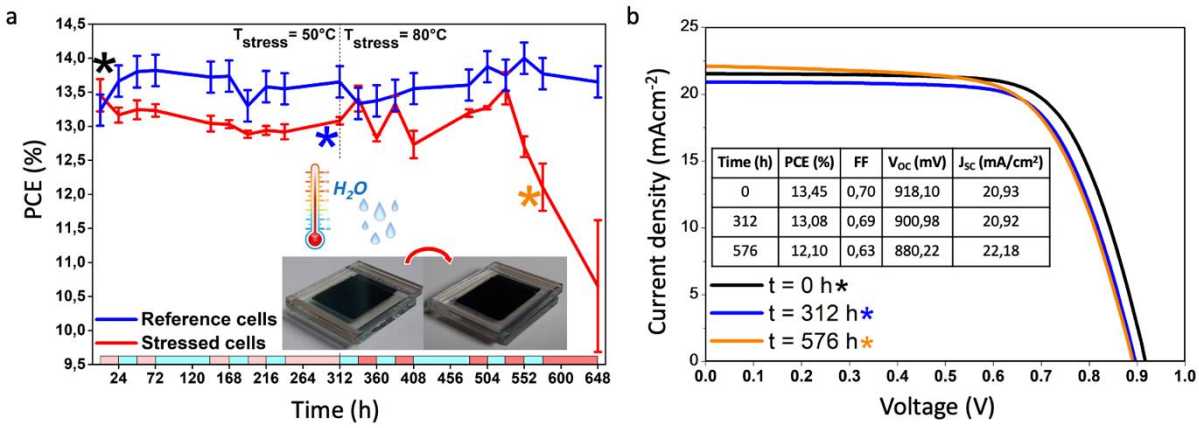

Time (h)	PCE (%)	FF	V_{OC} (mV)	J_{SC} (mA/cm²)
0	13,45	0,70	918,10	20,93
312	13,08	0,69	900,98	20,92
576	12,10	0,63	880,22	22,18

Figure 1 (a) Stability measurements monitoring the PCE versus time for a solar cell under thermal and humidity cycling (red line) compared to a reference cell kept in dark and ambient conditions (blue line). Note that the J-V measurements have been done immediately after the aging. Red sections at the bottom indicate stress periods (light red at 50° C and dark red 80° C) while light blue sections indicate recovery periods. Humidity kept constant of 72%. Three samples with the same architecture were measured each day, the differences in the PCE are indicated by error bars. In inset pictures of cells before (left) and after (right) stress. **(b)** Experimental current – voltage (J-V) curves measured at 1 sun illumination (AM1.5G spectrum) at t=0 h (fresh), after t=312h and t=576 h of aging as indicated by the asterisks. In inset solar cell parameters (PCE, FF, V_{OC} and J_{SC}) of the device for the J-V curves of Figure 1b.

During the recovering time the cell was kept in dark and in ambient conditions (RH=72%). At a first glance, during the overall aging, the C-PSCs show an average decrease in the power conversion efficiency (PCE) from an average value of 13.5% down to 10.6%. At a closer inspection, two behaviours can be revealed. If the devices are kept at 50°C, the PCE is stable. After switching to 80°C, the PCE remains stable for 230 hours, and then abruptly reduce to 20% of the initial values. On the contrary, reference cells, kept in ambient conditions and in the dark, are stable for the whole time window, further confirming the high stability of this device

architecture even in relatively high humidity conditions. **Figure 1b** shows the corresponding current-voltage (J-V) characteristics of the solar cells at 0 h, after 312 h and 576 h testing times, in forward scan. Upon aging, a remarkable reduction of the fill factor (FF) and of the open circuit voltage (V_{OC}) is observed, as summarized by the device parameters listed in the table in inset (see also **Table S1** and **Figure S1**). The trend of the FF mirrors the PCE, being constant for the first half of the cycle and decreasing in the second, while the reduction of the V_{OC} is uniform through all the aging cycle. In order to understand which device parameters could be mostly affected by thermal stress, we tracked and modelled device operation and parameters by developing a customised advanced fitting procedure. The equivalent circuit is based on single-diode model. At a given illumination, the current/voltage relationship is given by Equation 1 derived from the Shockley equation:

$$\boldsymbol{I = I_L - I_0\left[e^{\frac{q(V+R_S I)}{nk_BT}} - 1\right] - \frac{V+R_S I}{R_{SH}}} \quad (1)$$

where I_L, I_0, R_S, R_{SH}, q, n, k_B and T are the photocurrent, the saturation current of the diode, the series resistance, the shunt resistance, the electron charge, the ideality factor, the Boltzmann constant, and the temperature, respectively. It is worth recalling that the R_{SH} is usually related to the leakage current across the surfaces involving pinholes, grain boundaries, and charge recombination processes,[3] while the R_S is reflected in the voltage drops and related to the conductivity of the layers and interfaces.[22,23] The ideality factor is related to interfacial layers, transport, and recombination processes, directly affecting the R_{SH} and the V_{OC}.[24] Ideality factors for PSCs are usually between 1 and 2 (closer to 2 if severe trap-assisted recombination under dark condition happens).[25,26] To fit the J-V characteristics, the modelling program was implemented as schematized in **Figure S2**. First, due to the particular dependence on the current of Equation 1, we found zeros of the function (Equation 2) using

the bisection method. Then, we properly chose the initial values of the fitting parameters and their variation range, determining the final values for the least-square method.

$$f = I - I_L + I_0\left[e^{\frac{q(V+R_S I)}{nk_B T}} - 1\right] + \frac{V+R_S I}{R_{SH}} \qquad (2)$$

Notably, we could also randomly change the initial values of the parameters in order to leverage possible biasing throughout all the cycle, and to estimate the overall uncertainty in the final parameters. The set of parameters estimated for each cell results therefore reliable and unbiased, as it is independent of other results in the thermal aging cycle. From performing a "4-parameter-fit" – i.e. a procedure in which all the parameters (n, I_0, R_S, R_{SH}) are fitted - we conclude that the reverse saturation current is the most variable parameter, as it varies over an exponential scale (see also **Figure 2c**).

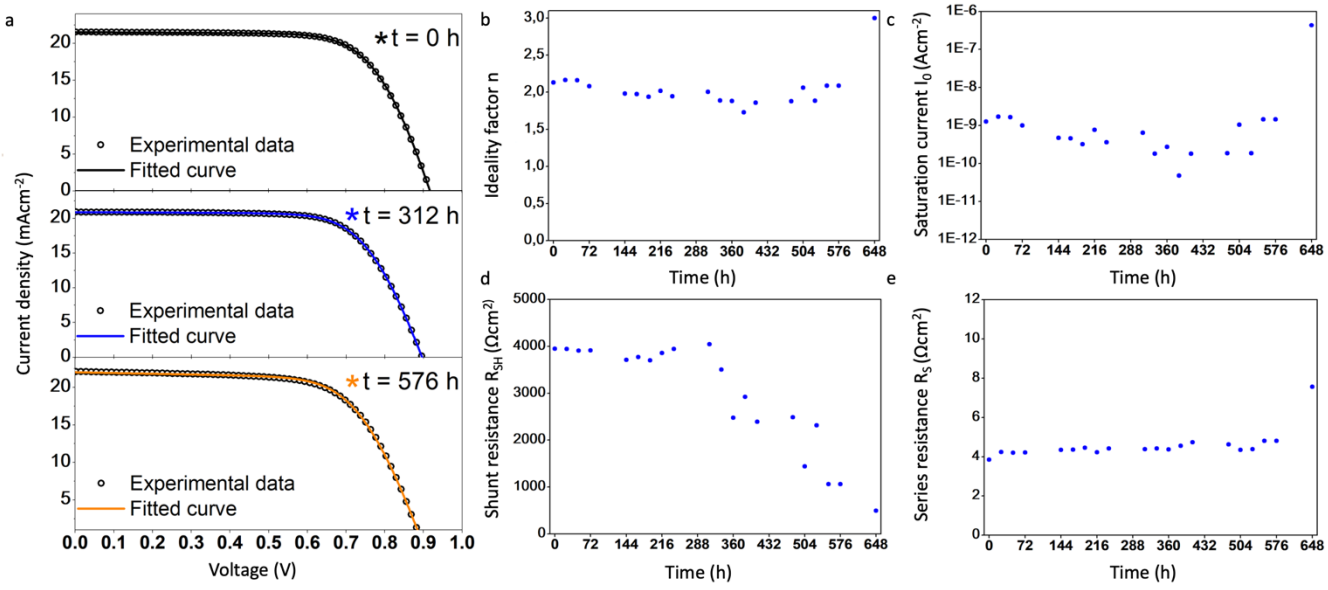

Figure 2 (a) Current-voltage characteristics curves at selected times (as in Figure 1b), superimposed with the fit. **(b-e)** Parameters extracted from data fitting using the model described in the text showing: **(b)** ideality factor (n), **(c)** reverse saturation current, **(d)** shunt

resistance and **(e)** series resistance. Note that the last point in the time window, corresponding to t = 648 h, is not at full convergence, probably due to the excessive degradation of the device.

To validate the robustness of the fit, we implemented an advanced version of the fitting procedure, consisting of a "3-parameter-fit" or a "4-parameter-fit". For the 3-parameter-fit (see **Figure S3**) we choose a fixed value for I_0 and retrieve the remaining parameters (n, R_S, RS_H). As **Figure S4** shows, the fitted curves match fairly well the experimental points, but the slight deviations are minimized when I_0 is fixed to the value determined from the 4-parameter fit ($J_0=10^{-11}$ Acm^{-2}, **Figure S4c**). **Figure 2a** shows the J-V characteristics curves at selected times (as in **Figure 1d**), superimposed with the fitted curves as resulting from the 4 parameter-fit. We observe that the fit is in a very good match with the experimental data, reproducing the whole set of data. **Figure 2(b-e)** represents the trend of the extracted parameters at different aging time in terms of: (b) n, (c) I_0, (d) R_{SH} and (e) R_S. From the fitting results (see **Table S2** for details about uncertainties), we can observe that: i) the ideality factor varies between 1.7 and 2.2, in agreement with;[25] ii) the reverse saturation current varies from 10^{-11} to 10^{-9} (due to the strong sensitivity of I_0 to recombination processes), as shown in Figure 2c; iii) R_{SH} is stable for the first part of the cycle and then decrease of two orders of magnitude; iv) R_S is barely affected throughout the entire cycle. The results point to a significant decrease in shunt resistance as the dominant factor responsible for device degradation. This suggests a minor effect of the aging on the bulk, while it indicates a severe impact on the device interfaces. Hereafter, we combine structural (X-ray Diffraction -XRD), morphological (scanning electron microscopy -SEM) and optical investigation to further elucidate the material properties before and after the aging test.

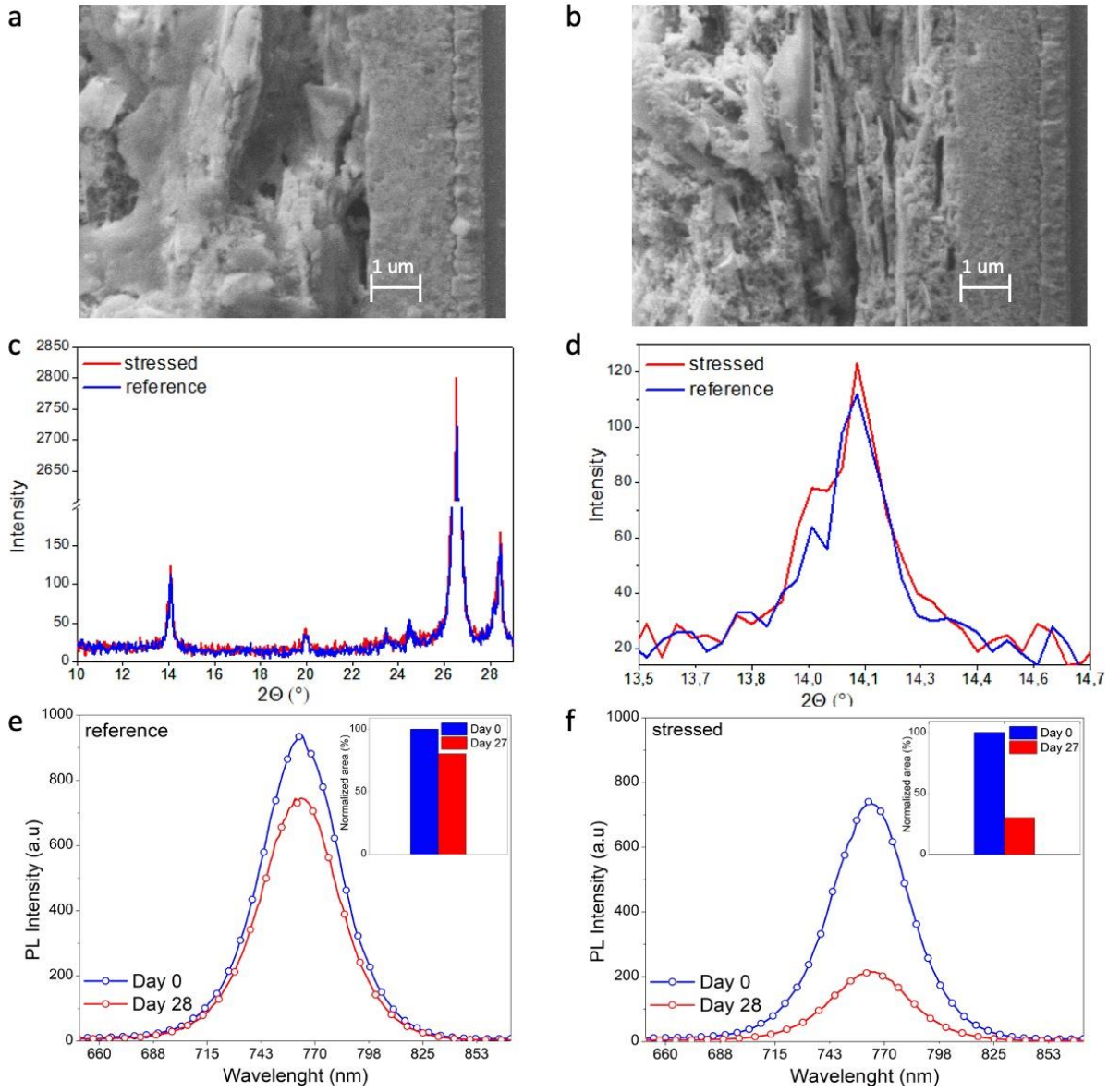

Figure 3. SEM images for the reference (a) and the stressed (b) cell. X-ray Diffraction pattern for the reference (blue line) and the stressed (red line) cell (c), zoom on the peak at 14° (d). Comparison between photoluminescence spectra at t=0 (blue line) and at t=648 h (red line) for the reference (a) and stressed cell (b). Excitation wavelength at 460 nm. The measurement is taken on the whole cell upon illumination from the bottom glass side.

Figure 3a and **3b** show the SEM images of the reference and stressed cells. From analyzing the SEM images in cross section, the perovskite bulk looks unchanged. **Figure 3c** and **3d**, shows the XRD patterns for the reference and the aged cell and a zoom at the region around

14°. At a first glance, the XRD trace of the aged device reveals no structural changes of the perovskite crystal structure. Remarkably, we can notice the absence of the peak at 12.4° related to PbI_2 phase (which would give a clear indication of material degradation). More in details, it is fair to recall that the perovskite active layer is made of methylammonium (MA) cation with the addition of 5-amino valeric acid (5-AVA) additive. It has been demonstrated (see Ref. 17) that 5-AVA templates the crystallization of the perovskite in the pores of mesoporous TiO_2 while its –COOH and $–NH_2$ groups interact with TiO_2 through hydrogen bonding, ensuring a better interfacial contact with the anode. In addition, it induces the formation an oriented interface where the $MAPbI_3$ phase has a marked preferential growth direction. This is evident from the increased reflections along the (110) and (220) directions speaking in favor for a preferred orientation along the (hk0) direction. Zooming on the XRD peak (see the new Fig. 3d), indeed, it is evident that the relative intensity of the main peak at 14.13° with respect to the peak at 14° changes. More in details, in the stressed cell both (002) and (004) increase in intensity, while the intensity of the (110) and (220) reflections decrease, losing the preferred orientation along the 0hk direction typical of the reference sample (see Ref. 17).

This suggests that thermal degradation affects the perovskite/TiO_2 contact by changing the crystal orientation at the very interface, reducing the marked preferential orientation and possibly influencing the quality of the interface itself (i.e. the trapping/detrapping). Overall, this observation enables us to assess that the thermal stress modifies the interface crystal orientation, enabling us disentangling the contributions of bulk vs interfaces.

To get a further understanding we also measured the reference and aged devices at time zero and after running the test, monitoring their photoluminescence (PL) signal. As such, PL offers a fingerprint of the quality of the perovskite layer and enables a qualitative prediction of the recombination mechanism.

Figure 3e and **3f** show the photoluminescence (PL) spectra of the cell at day 0 (blue line) compared to the signal registered for the same cell at day 28 (red line) for both the reference and the stressed solar cells, respectively. The reference cell shows a slight reduction of the PL intensity (19,6%) while the aged cell displays a more severe PL quenching (with a reduction of 69,9%). Despite the decrease in the PL signal could hide several concomitant effects, we suggest that it is associated with the reduced shunt resistance. This indicates an effect of the interfaces, rather than of the bulk. This is related to the fact that the PL experiment has been performed upon illuminating the device from the glass side. Considering that at 460 nm excitation wavelength the penetration depth is few hundreds of nanometers, we are mainly interrogating the perovskite layer which is infiltrated within the TiO_2 scaffold (500 nm thick, see "Experimental Section"). Therefore, the change in the PL is mainly due to perovskite/TiO_2 interface, excluding the bulk or the perovskite/ top contact interface. This interpretation is in line with the results of the fitting. The interpretation of degradation occurring at the perovskite/TiO2 interface is in line with the results of the fitting and of combined PL/XRD/SEM measurements, nevertheless a more complex scenario cannot be excluded at this stage. Associating degradation of solar cell efficiency to specific spatial locations will require more extended studies, including PL with excitation from both sides and simultaneous fitting of illuminated and dark IV curves.

Conclusions

In conclusion, our work sheds light on the degradation mechanisms of C-PSCs under thermal stress. C-PSCs are stable at temperature below 50° and up to 80° with limited operating time. Upon prolonged thermal stress, degradation takes place. From combined modeling, device

data and optical characterization, we can conclude that the main effect of thermal stress leads to a reduction of the shunt resistance. Despite this can be associated to both degradation of bulk perovskite and perovskite/contacts, PL and XRD analysis demonstrates that is the perovskite/TiO_2 interface which is mostly affected – mainly through a rearrangement of the interface orientation and interface crystallization. It is thus imperative to focus further work on the interface optimization as an effective strategy to overcome the instability issue and to bring this technology closer to marketability requirements.

Experimental Section

Solar cell fabrication

The carbon-based perovskite solar cell (C-PSC) consists of a multi-layered stack of compact titania (thickness around 50 nm), mesoporous titania (thickness around 500 nm), mesoporous zirconia (thickness around 1 μm), and porous carbon (thickness around 10–12 μm). The substrate consists of a 10 x 10 cm^2 plate of fluorine-doped tin oxide (FTO) coated glass (sheet resistance 7 ΩSq^{-1}, TCO22-7/LI, Solaronix). A laser pattern defines the electrodes areas. The FTO is cleaned with 1% aqueous solution of Hellmanex, acetone, and isopropanol respectively (15 min each) in an ultrasonic bath and subsequently dried in air. The compact TiO_2 layer is deposited by spray-pyrolysis on a hot-plate at 450°C, using a mask to protect cathode and contact areas. We spray 20 mL of titanium diisopropoxide bis (acetylacetonate) (75% in isopropanol, Sigma-Aldrich) diluted in absolute ethanol (1:160) and we anneal it for 30 min before allowing the sample to cool down. We design an array of 18 electrodes by screen-printing silver contacts (Elcosil SG/SP), mesoporous TiO_2 (Ti-nanoxide T165/SP – size 20 nm), mesoporous zirconia (Zr-nanoxide ZT/SP – size 20 nm), and carbon (Elcocarb B/SP size 30 nm, graphite flakes several microns in size). After printing the wet film, each screen-

printed layer is allowed to dwell for 10 min before drying at 120°C for 10 min, followed by an annealing step at 500°C (400°C for carbon) for 30 min, after a 30 min ramp. 5.76 µl of the perovskite precursor solution (made of methylammonium lead iodide perovskite precursor salt with a 5-aminovaleric acid iodide (5-AVAI) additive (Solaronix), see Ref. 28 for more details) is deposited. The infiltration of the perovskite ink is done using a customised semi-automated dispensing system. The samples annealed in an oven at 50°C dried for 60 min allowing perovskite crystallization within the porous matrix. The polyimide adhesive gasket is carefully peeled off, and the solar cells are cut. The devices are heated at 40°C and 75% R.H. for 150 h. Lastly, the solar cells are laminated with a 1.8 mm back glass and a 60 µm thick hotmelt gasket. The latter is cut out from Meltonix 1170 (Solaronix) to form a 1 mm wide barrier around the active area. Sealing is conducted at 95°C with a membrane press exerting a 1 atm pressure for 150 s.

Solar cell characterization

Photocurrent density voltage (J–V) curves were characterized with a Keithley 2400 source/metre and a Wavelabs solar simulator (model Sinus-70) providing a source of light with AM 1.5G spectral distribution. A black mask with an aperture smaller than the active area of the solar cell (0.2 cm^2) was applied on top of the cell. The light intensity was measured for calibration with a reference cell (RR-1001, ABET Technologies). No preconditioning protocol is used. Three samples with the same architecture were measured each day and immediately after the annealing or the period of recovery.

X-Ray diffraction measurements

X-ray diffraction measurements were performed using a D8 Advance diffractometer from Bruker (Bragg–Brentano geometry). Cu Kα was used as the X-ray source. Θ scans between 0° and 30° were collected with 700 steps with a step scan of 5s.

Photoluminescence measurements

Continuous wave (CW) photoluminescence measurements were performed using a spectrofluorimeter (Cary Eclipse Agilent) equipped with a lamp. Excitation wavelength was set at 460 nm and spectra were recorded between 650 nm and 870 nm

Scanning Electron Microscope measurements

A Zeiss EVO MA10 (Carl Zeiss, Oberkochen, Germany) scanning electron microscope equipped with LaB6 crystal for electrons generation was used for the morphologic study. The materials were supported on graphite bi-adhesives fixed on Al stubs and subsequently transferred in the SEM chamber. The measurements were performed under ultra-high vacuum at a working distance of 8.5 mm and with an electron generation voltage of 5 kV. The images were acquired in high vacuum through an Everhart-Thornley secondary electron detector

Supporting Information

Supporting Information is available from the Wiley Online Library or from the author.

Acknowledgements

The authors acknowledge the ‘HY-NANO’ project that has received funding from the European Research Council (ERC) Starting Grant 2018 under the European Union’s Horizon 2020 research and innovation programme (Grant agreement No. 802862).

Received: ((will be filled in by the editorial staff))

Revised: ((will be filled in by the editorial staff))

Published online: ((will be filled in by the editorial staff))

References

[1] F. De Angelis, *ACS Energy Lett.* **2017**, 2, 11, 2640–2641.

[2] Y. Zhang, M. Liu, G. E. Eperon, T. C. Leijtens, D. McMeekin, M. Saliba, W. Zheng, M. De Bastiani, A. Petrozza, L. M. Herz, M. B. Jhonston, H. Lin, H. J. Snaith**,** *Mater. Horiz.* **2015**, 2, 315-322.

[3] G. Schileo, G. Grancini, *J Phys Energy* **2020**, 2, 2, 021005.

[4] C. Roldán-Carmona, P. Gratia, I. Zimmermann, G. Grancini, P. Gao, M. Graetzel, M. Nazeeruddin, *Energy Environ. Sci.* **2015**, 8, 3550-3556.

[5] B. Conings, J. Drijkoningen, N. Gauquelin, A. Babayigit, J. D'Haen, L. D'Olieslaeger, A. Ethirajan, J. Verbeeck, J. Manca, E. Mosconi, F. De Angelis, H. G. Boyen, *Adv Energy Mater.* **2015**, 5, 15, 1500477.

[6] M. De Bastiani, G. Dell'Erba, M. Gandini, v. D'Innocenzo, S. Neutzner, A. R. S. Kandada, G. Grancini, M. Binda, M. Prato, J. M. Ball, M. Caironi, A. Petrozza, *Adv Energy Mater.* **2016**, *6, 2,* 1501453.

[7] D. Bryan, N. Aristido, S. Pont, I. Sanchez-Molina, T. Chotchunangatchaval, S. Wheeler, J. R. Durrant, S. A. Haque, *Energy Environ Sci*. **2016**, 9, 5, 1655–60.

[8] N. Rajamanickam, S. Kumari, V. K. Vendra, B. W. Lavery, J. Spurgeon, T. Druffel, M. K. Sunkara, *Nanotechnology*, **2016**, 27, 23, 235404.

[9] P. H. Joshi, L. Zhang, I. M. Hossain, H. A. Abbas, R. Kottokkaran, S. P. Nehra, M. Dhaka, M. Noack, V. L. Dalal, *AIP Advances* **2016**, 6, 11.

[10] N. Aristidou, I. Sanchez-Molina, T. Chotchuangchutchaval, M. Brown, L. Martinez, T. Rath, S. A. Haque, *Angew Chem. Int. Ed* **2015**, 127, 28, 8326–30.

[11] S. H. Chan, M. C. Wu, K. M Lee, W. C Chen, T. H. Lin, W. F Su, *J Mater Chem A.* **2017**, 5, 34, 18044–52.

[12] A. Agresti, S. Pescetelli, B. Taheri, A. Esaù Del Rio Castillo, L. Cinà, F. Bonaccorso, A. Di Carlo, *ChemSusChem* **2016**, 9, 2609-2619.

[13] C. Petridis, G. Kakavelakis, E. Kymakis, *Energy Environ. Sci.* **2018**, 11, 5, 1030–61.

[14] K. T. Cho, G. Grancini, Y. Lee, D. Konios, S. Paek, E. Kymakis, M. K. Nazeeruddin, *ChemSusChem* **2016**, 9, 21, 3040–4.

[15] N. Arora, M. I. Dar, A. Hinderhofer, N. Pellet, F. Schreiber, S. M. Zakeeruddin, M. Graetzel, *Science* **2017**, 358, 6364, 768–71.

[16] J. Xiang, Y. Li, F. Huang, D. Zhong, *Phys. Chem. Chem. Phys*. **2019**, 21, 32, 17836–45.

[17] G. Grancini, C. Roldán-Carmona, I. Zimmermann, E. Mosconi, X. Lee, D. Martineau, S. Narbey, F. Oswald, F. De Angelis, M. Graetzel, M. K. Nazeeruddin, *Nat Commun.* **2017**, 8, 1, 15684.

[18] L. Fagiolari, F. Bella, *Energy Environ. Sci*. **2019**, 12, 12, 3437–72.

[19] Y. Liu, C. Nie, X. Liu, X. Xu, Z. Sun, L. Pan, *RSC Adv*. **2015**, 5, 20, 15205–25.

[20] R. Po, C. Carbonera, A. Bernardi, F. Tinti, N. Camaioni, *Sol Energy Mater Sol Cells* **2012**, 100, 97–114.

[21] K. Domanski, J. P. Correa-Baena, N. Mine, M. K. Nazeeruddin, A. Abate, M. Saliba, W. Tress, A. Hagfeldt, M. Graetzel, *ACS Nano* **2016**, 10, 6, 6306–14.

[22] Y. Hu, E. M. Hutter, P. Rieder, I. Grill, J. Hanisch, M. F. Avguler, A. G. Hufnagel, M. Handloser, T. Bein, A. Hartschuh, K. Tvingstedt, V. Dyakonov, A. Baumann, T. J. Savenije, M. L. Petrus, P. Docampo, *Adv Energy Mater.* **2018**, 8, 16, 1703057.

[23] G. J. A. H. Wetzelaer, M. Scheepers, A. M. Sempere, C. Momblona, J. Avila, H. J. Bolink, *Adv Mater*. **2015**, 27, 11, 1837–41.

[24] D. Prochowicz, M. M. Tavakoli, A. Solanki, T. W. Goh, T. C. Sum, P. Yadav, *J Mater Chem C.* **2019**, 7, 5, 1273–9.

[25] W. Tress, M. Yavari, K. Domanski, P. Yadav, B. Niesen, J. P. Correa Baena, A. Hagfeldt, M. Graetzel, *Energy Environ Sci.* **2018**, 11, 1, 151–65.

[26] M. A. Cappelletti, G. A. Casas, A. P. Cedola, E. L. Peltzer, B. M.Soucase, *Superlattices Microstruct*. **2018**, 123, 338–48.

[27] S. Salamon, *Master Thesis*, PoliTO (Italy), December, **2019,** https://webthesis.biblio.polito.it/12999/1/tesi.pdf.

[28] A. Verma, D. Martineau, E. Hack, M. Makha, E. Turner, F. Nuesch, J. Heier, J. *Mater. Chem. C.* **2020**, 8, 6124-6135.

Table Of Contents

This work reveals the effect of thermal aging on state-of-the-art Carbon based -PSCs by imposing a prolonged (27 days) temperature cycling stress. By combining device characterization and advanced fitting modelling of the current–voltage characteristics of the C-PSCs, we provide a critical understanding revealing the robustness of the devices under accelerated thermal aging (up to 80°C) and the main device parameters affected.

Keyword: Perovskite solar cell, thermal stress, efficiency, solar cell stability, fitting

*Giovanni Pica, Matteo Degani, Giorgio Schileo, Alessandro Girella, Chiara Milanese, David Martineau, Lucio C. Andreani, Giulia Grancini**

Accelerated Thermal Aging Effects on Carbon-based Perovskite Solar Cells: a Joint Experimental and Theoretical Analysis.

TOC FIGURE (55mm broad x 50 mm high)